

Selective Selenate Adsorption on Cationated Amino-Functionalized MCM-41

Toshiyuki Yokoi,† Takashi Tatsumi,† and Hideaki Yoshitake*

Graduate School of Environment and Information Sciences, Yokohama National University, 79-7 Tokiwadai, Hodogaya-ku, Yokohama 240-8501

†Division of Material Sciences, Graduate School of Engineering, Yokohama National University, 79-5 Tokiwadai, Hodogaya-ku, Yokohama 240-8501

Received May 22, 2003; E-mail: yos@ynu.ac.jp

A large distribution coefficient and large sorption capacity were observed during selenate adsorption by cation (Fe^{3+}, Cu^{2+}, and H^+)-anchored diamino-functionalized MCM-41. Moreover, these synthetic adsorption media showed excellent selectivity for selenate sorption in the presence of other anions. In a pure potassium selenate solution, the distribution coefficients, K_d, exceeded 200000 when [selenate] < 25 mg in 1 g of these adsorbents (i.e., when the coverage of selenate < 0.4). The adsorption capacities of these three adsorption media were 117, 83.0, and 123 mg (g-adsorbent)$^{-1}$, respectively, with the Fe and Cu centers having the capacity to bind 1.5 and 1.1 selenate anions on average. Tests on mono- (N-), di- (NN-), and triamino- (NNN-) functionalized MCM-41 showed that the diamino-functionalized varieties exhibited the largest value for K_d when cationated by Fe^{3+} and Cu^{2+}. In the case of Fe/NN-MCM-41, diamino-functionalized MCM-41 cationated by Fe^{3+}, the degree of inhibition caused by coexisting SO_4^{2-} was much lower than the value reported for aluminum oxide. Cu/NN-MCM-41 showed the largest resistance to inhibition by Cl^-. For the adsorbents that we tested, the effects of coexisting nitrate were smallest for these three anions. The local structure of the adsorption center in Fe/NN-MCM-41 was analyzed by EXAFS spectroscopy.

Since the discovery of well-ordered hexagonal mesoporous silica,[1–3] considerable efforts have been made to expand the range of applications of silica materials in many fields of materials chemistry by utilizing their high surface area, controllable pore size, and narrow pore size distribution. These structural characteristics are attractive for developing adsorbents for toxic ions in the environment. Since silica is generally believed to interact weakly with molecules and ions, functionalization of its surface is essential to obtain a desirable adsorption capacity. A high density of silanol groups[4] aids in fixing a large amount of active organosilanes for adsorption on a silica surface.

Designs that utilize the adsorption sites on silica, with their high surface areas accompanied by mesopores, are promising ways of immobilizing ions in contaminated water. The direct interaction of Hg^{2+} with an –SH pair has been proposed for the adsorption of mercury on mercaptopropyl-functionalized mesoporous silicas,[5–8] while improved capacity has been demonstrated by using a 1-allyl-3-propylthiourea group instead of a mercaptopropyl group.[9] Divalent cations, such as Cu^{2+}, Cr^{2+}, and Ni^{2+}, which are also toxic and often emitted into wastewater, are adsorbed to a greater extent by aminopropyl-functionalized SBA-15 than by mercaptopropyl groups on the same kind of mesoporous silica.[10]

Environmentally toxic oxyanions, such as arsenate and chromate, are negatively charged and the central atoms are surrounded by the coordination environment of T_d oxygen. This leads to difficulties in selective adsorption from solutions containing other common oxyanions, such as sulfate and phosphate. On the other hand, these toxic anions are often found in groundwater and cause serious problems to the quality of drinking water from wells. Recently, it has been demonstrated that several kinds of amino-functionalized SBA-1,[11,12] MCM-41,[12] and MCM-48[13] show considerable adsorption capacity. Although complete removal (<1 ppb) of toxins can be achieved in an aqueous solution saturated with carbonate, considerable inhibition due to other anions (SO_4^{2-}, Cl^-, NO_3^-, etc.) can occur during the treatment of contaminated groundwater because the interaction between the amino groups and the oxyanions is largely ionic and the chemical differences between the ions have hardly any effect on the formation of bonds. Cu(II)[14,15] and Fe(III)[15] were anchored by amino-functionalized MCM-41, which was prepared by grafting aminosilanes onto MCM-41. The resulting solids showed a large adsorption capacity for arsenate.

Among oxyanions with the T_d structure, selenate is particularly significant in environmental science because of its toxicity towards animals[16–21] and its mobility in the soil. The adsorption on inorganic oxides,[22,23] biological reactions[24–26] and chronic toxicity[27] have also been studied to gain a better understanding of the potential hazards of selenate. Groundwater pollution has also been reported.[28] Environmental regulations for selenate are usually strict, and its almost complete removal is needed to obtain potable water from a contaminated source. It should, however, be considered that the most abundant anion species in fresh water is usually sulfate, whose geometrical and electronic structures are similar to selenate, which makes separation difficult. In the literature, aluminum oxide- and iron ox-

Published on the web November 15, 2003; DOI 10.1246/bcsj.76.2225

ide-coated sands were evaluated for the removal of selenate from water in a few studies[29,30] in which the adsorption capacity did not exceed 0.60 mg Se/g-adsorbent and a significant suppression of adsorption was observed in the presence of sulfate.

It is a challenging theme for functionalized porous materials to achieve one of the most difficult separations in relation to toxic oxyanions, SeO_4^{2-}/SO_4^{2-}. In the present study, we investigated the removal of selenate by comparing (1) several different cation centers, Fe^{3+}, Co^{2+}, Ni^{2+}, Cu^{2+}, and H^+, (2) the number of amino groups in the organic chain in functionalized MCM-41 and (3) the suppression of selenate uptake caused by coexisting sulfate and other anions. The structure of the adsorption sites that showed a specific interaction with selenate was analyzed by EXAFS spectroscopy.

Experimental

Chemicals. Tetraethyl orthosilicate (TEOS, reagent grade) and dodecyltrimethylammonium bromide (DTMABr, purity > 98%) were commercially available. Trimethylammonium hydroxide (TMAOH, Aldrich) was used as received. 3-Aminopropyltrimethoxysilane ($H_2NCH_2CH_2CH_2Si(OCH_3)_3$) and *N*-[3-(trimethoxysilyl)propyl]ethylenediamine ($H_2NCH_2CH_2NHCH_2CH_2CH_2Si(OCH_3)_3$) were purchased from Tokyo Kasei Kogyo Co., Ltd. N^1-[3-(trimethoxysilyl)propyl]diethylenetriamine ($H_2NCH_2CH_2HNCH_2CH_2NHCH_2CH_2CH_2Si(OCH_3)_3$) was obtained from Aldrich. Potassium selenate (K_2SeO_4, Pr.G.) was purchased from Wako Pure Chemical Industries Ltd.

Preparation of Mesoporous Silicas. TEOS, DTMABr, and TMAOH were mixed in water and the solution was stirred for 4 h at room temperature. The composition of the gel mixture was Si:DTMABr:TMAOH:H_2O = 1:0.6:0.3:60. The resulting gel was transferred into a Teflon bottle in an oven at 373 K. After 10 days, white precipitates were filtered and dried at 393 K. This as-synthesized powder was heated in a convex oven, where the temperature rose at 1 K min^{-1} up to 813 K and then remained constant for 4 h, to obtain MCM-41. A well-known (100), (110), (200), and (210) reflection pattern indicating the hexagonal *p6mm* structure was confirmed by X-ray diffraction measurements. The BET specific surface area and pore sizes, as determined by a nitrogen adsorption experiment, were 1280 $m^2\,g^{-1}$ and 2.9 nm, respectively.

Functionalization by Aminosilanes and Anchoring Cations. The MCM-41 that we obtained was dehydrated at 423 K in a vacuum to remove any water molecules adsorbed on the surface, and was then stirred vigorously in toluene containing one monolayer equivalent amount (1.0 per 1 nm^2) of 3-aminopropyltrimethoxysilane, *N*-[3-(trimethoxysilyl)propyl]ethylenediamine, or N^1-[3-(trimethoxysilyl)propyl]diethylenetriamine. These solutions were heated to 383 K in dry nitrogen for 6 h. The resulting powder was collected by filtration, washed with 2-propanol for 2 h and dried at 373 K. 100 mg of the powder was then stirred in 100 mL of 0.1 M HCl for 6 h without heating. This process converted the amino groups into salts. These mono-, di-, and triamino-functionalized MCM-41 chlorides are denoted by H/N-, H/NN-, and H/NNN-MCM-41, respectively. Nitrogen-adsorption experiments revealed that their respective BET surface areas were 1040, 586, and 481 $m^2\,g^{-1}$ with pore sizes of 2.8, 2.6, and 2.5 nm. N-contents determined by elemental analysis were 1.5, 2.8, and 3.5 mmol g^{-1} for H/N-, H/NN-, and H/NNN-MCM-41, respectively. The amino-functionalized MCM-41 samples were alternatively treated with 0.1 M 2-propanol solutions of $FeCl_3$, $CoCl_2$, $NiCl_2$, or $CuCl_2$; the powders were stirred in the chloride solutions at room temperature for 2 h, washed twice with 2-propanol and dried in an oven. These cation-anchored silicas are denoted as Fe/NN-MCM-41, Co/NN-MCM-41, etc. A small degradation of the mesostructural order of the powders was observed in the X-ray diffraction patterns and pore-size distributions. Their BET surface areas, however, remained as 380, 580, 284, and 588 $m^2\,g^{-1}$ for Fe/, Co/, Ni/, and Cu/NN-MCM-41, respectively.

Adsorption Experiments. The standard procedure that we adopted for the adsorption experiments was as follows. A 50 mg quantity of the functionalized MCM-41 was stirred for 10 h in 10 mL of an aqueous solution of K_2SeO_4. The solution was filtered to remove the solids and analyzed by induced coupled plasma (ICP) spectrometry. Typical pH values of the starting solutions were 6.1–6.5; after adsorption, these had decreased by ca. 0.3 (Co^{2+} and Ni^{2+}), 1.2–2.2 (Cu^{2+}), and 3.2–3.6 (Fe^{3+}), depending on the initial concentration of the selenate. Under these pH conditions, the dominant selenate species in aqueous solution is SeO_4^{2-} ($pK_{a_2} = 1.7$). A pH buffer was not used because the coexistence of other anions can influence the adsorption of selenate. The composition of the resulting powder was determined by ICP and CHN elemental analyzes.

The EXAFS spectra of the Fe and Se K-edges were measured on a BL-10B at the Photon Factory, High Energy Accelerator Research Organization, Tsukuba, Japan (Proposal #2001G133), using a ring energy of 2.5 GeV and a stored current of around 300–450 mA. A Si(311) channel cut monochromator was used. A transmission mode with detection using gas ion chambers was employed. The EXAFS spectra were acquired five times under the same measuring conditions, and the average $\chi(k)$ was calculated from the extracted spectra. The data were processed using a REX 2000 (Rigaku Co.) program. The EXAFS oscillation was extracted by fitting a cubic spline function through the post edge region. After normalization using the McMaster tables, the k^3-weighted EXAFS oscillation, $k^3\chi(k)$, in the 3–13 $Å^{-1}$ (1 $Å^{-1}$ = 10 nm^{-1}) region was Fourier transformed into a radial distribution function. The amplitudes and phase-shift functions for Fe–N, Fe–Cl, Fe–Se, and Se–O bonds were calculated by FEFF 7.02 code. A curve-fitting analysis was carried out between 4 and 12 $Å^{-1}$ in the *k*-space of the inversely Fourier transformed spectra (from FT filtered at $0.77 < r < 3.65$ Å and $0.89 < r < 3.34$ Å for Fe K- and Se K-edges, respectively, where 10 Å = 1 nm).

Results and Discussion

Adsorption Behaviour of Selenate in the Absence of Inhibiting Anions. Since the almost complete adsorption of selenate is necessary to meet strict environmental regulations, the distribution coefficient between the solid and liquid phases, K_d = (amount of selenate in 1 g adsorbent)/(amount of selenate in 1 g solution), is critically important in evaluating the performance of adsorbates for toxic oxyanions, such as Se, As, Cr(VI), and Mo(VI). K_d is plotted against the amount of adsorption in Fig. 1. The coefficients decreased according to the SeO_4^{2-} coverage. Fe/, Cu/, and H/NN-MCM-41 achieved $K_d >$ 200000, i.e. the amount of selenate in solution is less than 1 ppb, when the $[SeO_4^{2-}]_{ads} < 25$ mg (g-adsorbent)$^{-1}$, whilst the K_d found for Co/ and Ni/NN-MCM-41 did not exceed 10^3. Saturation of the adsorption is highlighted by the occurrence of a vertical decrease in this plot, which we have marked out approximately with dotted lines. This is observed at around $K_d = 10^2$ for Fe/, Co/. Cu/, and H/NN-MCM-41, implying

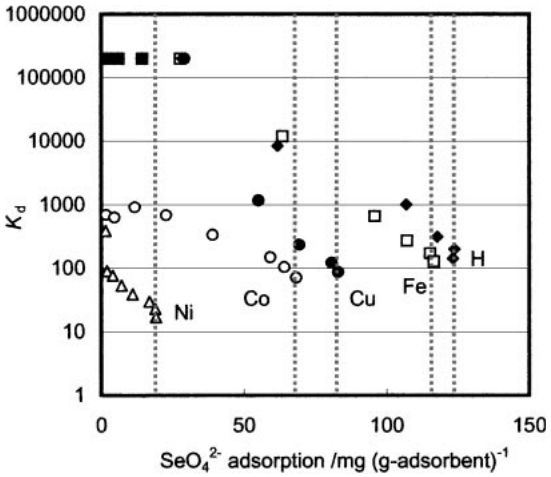

Fig. 1. Distribution coefficient versus amount of adsorption. Vertical broken lines indicate adsorption capacity. The detection limit of ICP (<1 ppb) confines the K_d higher than 200000. Experimental conditions: $C_{initial}$ (SeO_4^{2-}): 10.7–1400 ppm, adsorbent: 50 mg, solution: 10 mL, adsorption time: 10 h, adsorption temperature: 298 K.

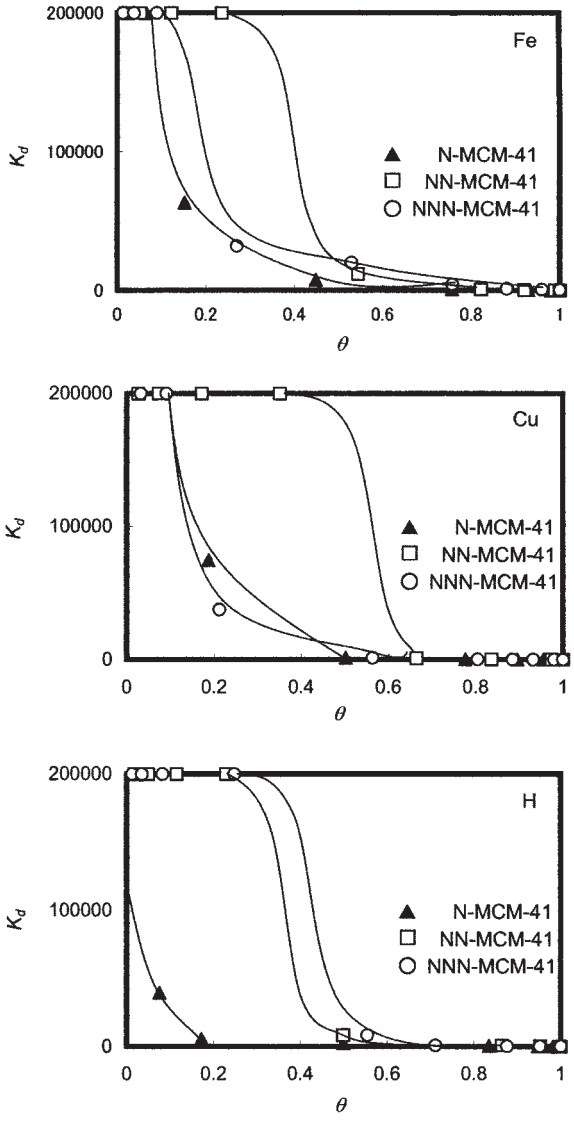

Fig. 2. Distribution coefficient versus coverage of selenate. The functional groups are compared for each cation. N-MCM-41 (▲), NN-MCM-41 (□), and NNN-MCM-41 (○). Experimental conditions: $C_{initial}$ (SeO_4^{2-}): 10.7–1400 ppm, adsorbent: 50 mg, solution: 10 mL, adsorption time: 10 h, adsorption temperature: 298 K.

that these adsorbents show a large affinity for selenate, even near to full coverage.

The different kinds of ligands in the functional groups of the MCM-41 are compared in plots of K_d versus the coverage of selenate in Fig. 2. In the case of the diamino-ligand, a sudden decrease of K_d occurred at $\theta = 0.4$–0.6, implying that the mode of adsorption changes at around half coverage. On the other hand, the decrease in K_d starts at a much earlier stage of the adsorption (θ = ca. 0.1) when the monoamino ligand is used to anchor the cations. K_d for Fe/ and Cu/NNN-MCM-41 show a similar behaviour to those of Fe/ and Cu/N-MCM-41, respectively. The finding that the strongest adsorption occurs at cation sites anchored by diamino-functionalized MCM-41 suggests that, although Fe^{3+} and Cu^{2+} can coordinate to amine ligands in several ways, those anchored by an ethylenediamine type ligand are the most strongly bound to selenate. The K_d–θ plot for H/NNN-MCM-41 almost replicates that of the H/NN-MCM-41, although the maximum adsorption for H/NNN-MCM-41 is considerably larger than that for H/NN-MCM-41 (Table 1). The large adsorption capacity with the small K_d value in the case of H/NNN-MCM-41 reveals that, over a large portion of the coverage, selenate is weakly bound to the surface site.

The maximum adsorption values, which approximately equate to the adsorption capacity, and the stoichiometries are summarized in Table 1. The coordination of Fe^{3+} increases with the number of amino groups, whereas MCM-41 with an ethylenediamine type-ligand anchors the largest amount of Cu^{2+}. The difference between the cations is probably caused by the stabilization constants of the amino ligands, which are not yet fully elucidated. The order of the adsorption capacities reflect the amount of the respective cations that are present, i.e. NNN- > NN- > N- for Fe^{3+} and NN- > N- > NNN- for Cu^{2+}. On the other hand, for H^+, the adsorption capacity simply increased with the number of amino groups. In our experiments, 173 mg (g-adsorbent)$^{-1}$ is the maximum capacity. This value is 160-times larger than the capacity reported for Al(Ⅲ) and Fe(Ⅲ) oxide-coated sands: <0.60 mg Se/g-adsorbent (= 1.1 mg SeO_4^{2-}/g-adsorbent).[29,30]

The average coordination ratios, Se/M, are also listed in Table 1. In Fe/N- and Fe/NN-MCM-41, Se/Fe is almost 1.5, suggesting that half of the Fe coordinates to two SeO_4^{2-} and the other half coordinates to one SeO_4^{2-}, while a 1:1 complex is implied for Se coordinated Cu/N- and Cu/NN-MCM-41. No specific structure can be proposed from the stoichiometry of Se to H in H/N-, H/NN-, and H/NNN-MCM-41: 2.3–2.7 N bound to one selenate. Since adsorption on protonated functionalized MCM-41 occurs largely by ion exchange, the charge balance and accessibility of the oxyanion to the organic groups may determine the Se/N ratio.

The N/Fe ratio in Fe/NN-MCM-41 before adsorption was

Table 1. Maximum Adsorption and Stoichiometries of Selenate on M/N-, M/NN-, and M/NNN-MCM-41

	M content[a)]	Adsorption[b)]	Se/N	Se/M	N/M
Fe/N-MCM-41	0.41	93.2	0.50	1.6	3.2
Cu/N-MCM-41	0.48	75.9	0.43	1.1	2.6
H/N-MCM-41	—	80.0	0.43	—	—
Fe/NN-MCM-41	0.55	117	0.39	1.5	3.8
Cu/NN-MCM-41	0.52	83.0	0.31	1.1	3.5
H/NN-MCM-41	—	123	0.37	—	—
Fe/NNN-MCM-41	1.03	159	0.38	1.1	2.9
Cu/NNN-MCM-41	0.34	66.7	0.14	1.4	10
H/NNN-MCM-41	—	173	0.39	—	—

a) mmol/(g-adsorbent). b) (mg-SeO_4^{2-})/(g-adsorbent). Experimental conditions: $C_{initial}$ (SeO_4^{2-}): 1400 ppm, adsorbent: 50 mg, solution: 10 mL, adsorption time: 10 h, adsorption temperature: 298 K.

Table 2. Inhibition of Selenate Adsorption on M/NN-MCM-41 (M = Fe, Co, Ni, Cu, and H) by Coexistence of Sulfate, Chloride and Nitrate

	SO_4^{2-}			Cl^-			NO_3^-		
	$C_{initial}$ /ppm	K_d	Removal /%	$C_{initial}$ /ppm	K_d	Removal /%	$C_{initial}$ /ppm	K_d	Removal /%
Fe^{3+}	0 (0)	>200000	100	0 (0)	>200000	100	0 (0)	>200000	100
	203 (2.8)	>200000	100	121 (1.7)	2267	92	146 (2.0)	>200000	100
	1014 (14)	2381	92	607 (8.5)	1791	90	730 (10)	31678	99
Co^{2+}	0	907	82	0	907	82	0	907	82
	203	446	69	121	688	78	146	571	74
	1014	52	21	607	471	70	730	382	66
Ni^{2+}	0	77	28	0	77	28	0	77	28
	203	39	16	121	62	24	146	64	24
	1014	22	10	607	50	20	730	48	20
Cu^{2+}	0	>200000	100	0	>200000	100	0	>200000	100
	203	1585	89	121	88859	100	146	>200000	100
	1014	167	46	607	3229	94	730	>200000	100
H^+	0	>200000	100	0	>200000	100	0	>200000	100
	203	800	80	121	12010	98	146	86687	100
	1014	44	18	607	1533	89	730	2623	93

The distribution coefficient (K_d) and removal (in %) of selenate are shown for initial concentration of inhibitors ($C_{initial}$). Experimental conditions: $C_{initial}$ (SeO_4^{2-}): 71.3 ppm, adsorbent: 50 mg, solution: 10 mL, adsorption time: 10 h, adsorption temperature: 298 K. The numbers in parentheses are the [inhibiting anion]/[SeO_4^{2-}] in the initial solution.

3.8, which agrees completely with the N/Fe ratio calculated in Table 1. N/Cu before exposure to the selenate solution was 3.6, which is also nearly unchanged, i.e. 3.5 after the full-coverage adsorption (Table 1). This agreement strongly suggests that the metal cations are fixed largely by a stable $M(en)_2$ type coordination structure and that adsorption occurs accompanied by an exchange reaction of Cl^- and selenate in order to balance the charge.

Inhibition by Sulfate, Chloride and Nitrate. The coexistence of anions, such as chloride and sulfate, has been an important issue when investigating the adsorption, the toxicity and the separation of selenate, because these anions are widely found in the environment and in concentrations that are orders of magnitude larger than the environmental regulations for selenate (usually <10 ppb). Carbonate can enhance the adsorption of oxyanions, such as selenate and sulfate, on the surface of goethite.[31] Furthermore, a comparison between the latter two anions has been carried out.[32,33] In the case of aluminium oxide, the adsorption of selenate was reduced by 70% in the presence of sulfate at a ratio of $SO_4^{2-}/Se(VI) = 1.8$.[29] The effects of sulfate on the acute toxicity of selenate are disputable,[34] while competition between these anions for active transport across cell membranes has been reported.[35] We also measured K_d for selenate adsorption in the presence of sulfate, chloride, and nitrate ions, as shown in Table 2. In the presence of sulfate at $SO_4^{2-}/Se(VI) = 2.8$, no inhibition was observed for Fe/NN-MCM-41, while reductions of 16, 43, 11, and 20% with respect to the removal of selenate were observed for Co/, Ni/, Cu/, and H/NN-MCM-41, respectively. The influence of coexisting ions on these synthetic adsorbents is much lower than on aluminium oxide (70% reduction at $SO_4^{2-}/Se(VI) = 1.8$[29]). Fe/NN-MCM-41 showed the largest resistance to sulfate inhibition over the $SO_4^{2-}/Se(VI)$ range that we investigated. At $SO_4^{2-}/Se(VI) = 14$ there was only an 8% reduction on Fe/NN-MCM-41, while decreases of 74, 64, 54, and 82% were observed in Co/, Ni/, Cu/, and H/NN-MCM-41, respectively. It should be noted that the largest absorption capacity was found in proton anchored NN-MCM-41 in the pure selenate solution

(Table 1), though suppression by sulfate is also the largest among the cations.

On the other hand, the influence of chloride was the lowest on Cu/NN-MCM-41 (6% reduction at $Cl^-/Se(VI) = 8.5$). At the same concentration, the degree of removal decreased by 10, 15, 29, and 11% on Fe/, Co/, Ni/, and H/NN-MCM-41, respectively. The inhibition caused by nitrate was also weaker than that caused by sulfate. Very little suppression was observed on Fe/ and Cu/NN-MCM-41, while Co/ and Ni/NN-MCM-41 showed suppressions comparable to those seen with chloride.

In terms of arsenate adsorption, Fe/NN-MCM-41 is less influenced by the coexistence of sulfate and chloride than by any other cations.[15] In selenate adsorption, the suppression due to chloride is lowest for Cu/NN-MCM-41, though sulfate inhibition is at a minimum on Fe/NN-MCM-41. Although the resistances of Co/NN-MCM-41 in arsenate adsorption were similar to Fe/NN-MCM-41,[15] suppression is significant in selenate adsorptions. Results from a study that claims that pre-adsorbed selenate does not affect cobalt adsorption on γ-Al_2O_3[36] implies that the interaction of Co^{2+} and selenate on the surface is not strong.

The difference in the inhibiting behavior on the various adsorbents demonstrates that uncoordinated ligands (namely, $H_3N^+\cdots$ and $-N^+H_2\cdots$) in Fe/, Co/, Ni/, and Cu/NN-MCM-41 bring about only minor effects on the adsorption of selenate, even if they do really exist.

Local Structure of Fe in Selenate on Fe/NN-MCM-41. Tris(ethylenediamine)iron(III) sulfate has been known as a $[Fe(en)_3]$ complex in a homogeneous solution,[37] implying that all three coordinations, i.e. $[Fe(en)]$, $[Fe(en)_2]$, and $[Fe(en)_3]$ type complexes, are possible, depending on the surface density of the amino groups. A figure of N/Fe = 3.8 (calculated in Table 1) supports the notion that $[Fe^{3+}(en)_2]$ is the major coordination structure in Fe/NN-MCM-41 that adsorbs selenate.

The Fe K-edge XANES spectra of Fe/NN-MCM-41 prior to and following selenate adsorption are shown in Fig. 3. The characteristic preedge peaks attributed to the 1s–3d transition[38,39] appear around 7110 eV. The peak maximum was found at 7109.9 eV in Fe/NN-MCM-41. On the other hand, this can be deconvoluted into two peaks at 7109.6 and 7110.9 eV in Fe/NN-MCM-41 after adsorbing selenate, suggesting two distinct states of Fe after adsorption. This result is consistent with a mixture of 2Se–Fe and Se–Fe surface complexes, which can explain the Se/Fe ratio given in Table 1. A contribution from the $[Fe^{3+}(en)_2]Cl^-{}_3$ that is not bound to the selenate is also possible.

Figure 4 shows $k^3\chi(k)$ EXAFS, the radial distribution function and the result of a curve-fitting analysis for the Fe K-edge EXAFS of Fe/NN-MCM-41 after fully adsorbing selenate. The amplitude of EXAFS oscillation when $k > 7$ Å^{-1} was enlarged and a large phase shift occurred after adsorption, suggesting the formation of a new chemical bond at a larger r than the bond lengths of Fe–N or Fe–Cl. Before adsorption, a strong peak around 1.9 Å, attributed to the Fe–Cl shell, is accompanied by a shoulder peak at around 1.3 Å in the Fourier transform. The coordination number of the Cl shell, N(Fe–Cl), was calculated to be 2.1, with a distance r(Fe–Cl) of 2.24 Å.[15] The small shoulder peak is assigned to the Fe–N shell

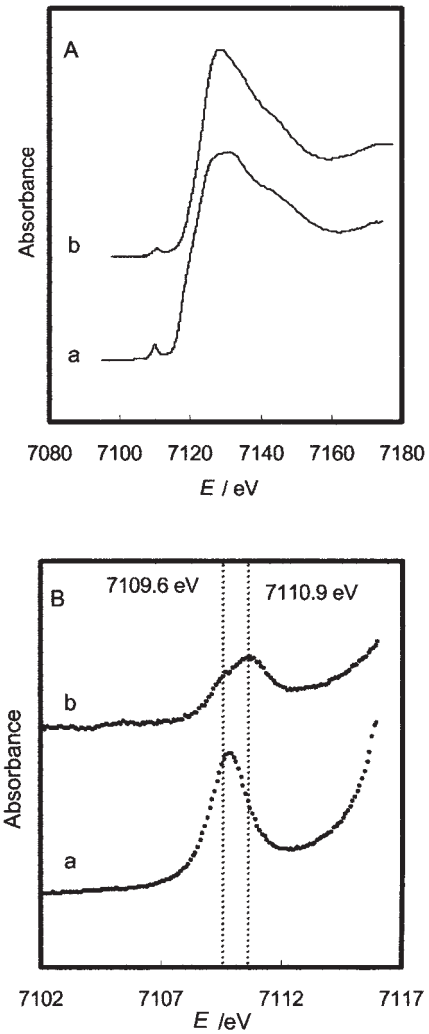

Fig. 3. Fe K-edge XANES of Fe/NN-MCM-41 (a) and Fe/NN-MCM-41 absorbing selenate (b). The preedge region in A is magnified in B. Selenate was fully adsorbed.

with N(Fe–N) = 3.3 and r(Fe–N) = 1.92 Å. Thus, in the proposed local structure of the adsorption site prior to selenate adsorption, the Fe is bound to two Cl^- at 2.24 Å and to four nitrogen atoms on the amine group at 1.92 Å on the surface. The latter proposal is consistent with the N/Fe stoichiometry (= 3.8) that was indicated by the elemental analysis.[15]

The intensity of the peak for Fe–Cl significantly decreased after the selenate adsorption in the Fourier transform. N for Fe–N and Fe–Cl was calculated to be 3.8 and 0.41, respectively. A value of N below unity for Fe–Cl implies the loss of chemical bonds. The result of the curve fitting is summarized in Table 3. The bond lengths remain nearly the same, 2.00 and 2.26 Å for Fe–N and Fe–Cl, respectively. A new peak at around 2.8 Å in the Fourier transform was assigned to the Se shell. The R factor was as small as 4% in the fitting with the parameters N(Fe–Se) = 0.93 and r(Fe–Se) = 3.27 Å. Taken together, these results suggest that the original Fe complex was $[Fe^{III}(en)_2]Cl^-{}_2$, probably accompanied by a third Cl^- in the outer sphere to neutralize the charge. The adsorption of selenate resulted in a displacement of Cl^- ions in the inner sphere, resulting in one of the selenate ions being bound to the Fe

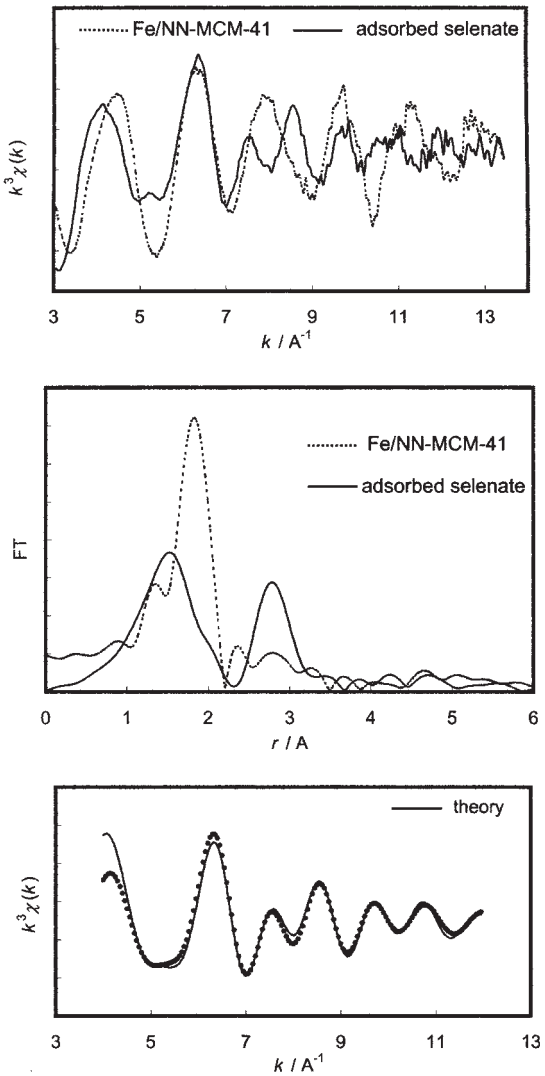

Fig. 4. EXAFS oscillation, Fourier transform, and curve fitting result (dot: experiment and line: theory) of Fe K-edge EXAFS of Fe/NN-MCM-41 fully adsorbing selenate. In the EXAFS oscillation and Fourier transform, the data for Fe/NN-MCM-41 prior to selenate adsorption are shown for comparison.

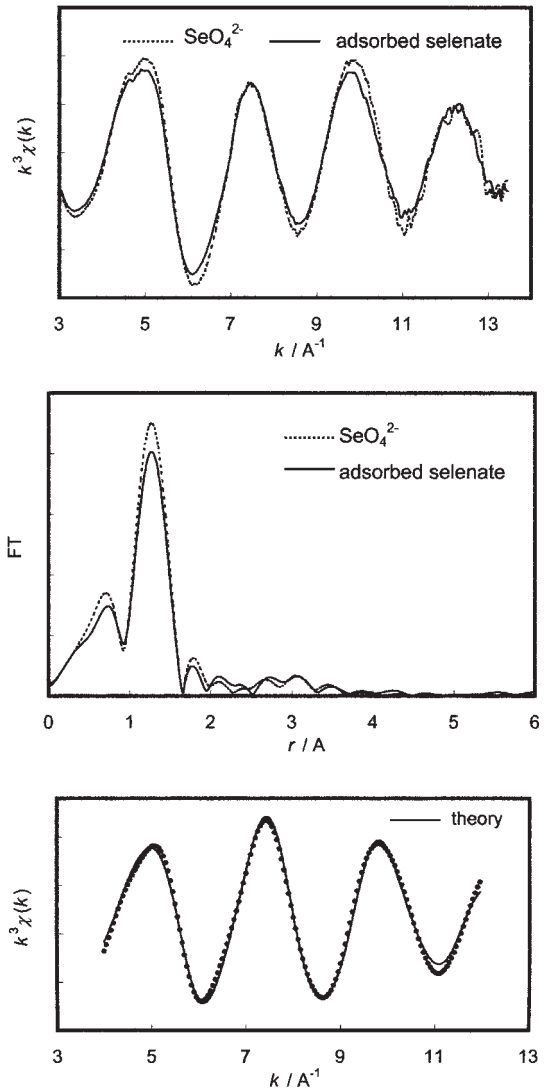

Fig. 5. EXAFS oscillation, Fourier transform, and curve fitting result (dot: experiment and line: theory) of Se K-edge EXAFS of selenate adsorbed on Fe/NN-MCM-41. In the EXAFS oscillation and Fourier transform, the data measured for an aqueous solution of SeO_4^{2-} are shown for comparison.

Table 3. EXAFS Curve-Fitting Results for Selenate Adsorbed on Fe/NN-MCM-41

	N	r/Å	σ/Å	R factor/%
		Fe K-edge		
Fe–N	3.8 ± 0.7	2.00 ± 0.03	0.096 ± 0.02	
Fe–Cl	0.41 ± 0.2	2.26 ± 0.03	0.066 ± 0.01	4.29
Fe–Se	0.93 ± 0.2	3.27 ± 0.04	0.062 ± 0.01	
		Se K-edge		
Se–O	3.7 ± 0.7	1.65 ± 0.02	0.063 ± 0.01	0.81
Se–Fe	0.43 ± 0.2	3.28 ± 0.04	0.087 ± 0.02	

1 Å = 0.1 nm.

center. The coordination number is smaller than that for Se/Fe determined by the ICP elemental analysis shown in Table 1. This disagreement can be explained by the existence of a large or disordered Se–Fe bond.

Little difference is found in $k^3\chi(k)$ EXAFS of the Se K-edge prior to and following selenate adsorption, as shown in Fig. 5. As a consequence, the Fourier transforms are almost the same. After considering the Se–Fe shell, the R factor in the curve fit-

ting was improved from 1.8 to 0.8%, when the calculation gave $N = 0.43$ and $r = 3.28$ Å for this shell. The bond length shows good agreement with the r(Fe–Se) determined in the Fe K-edge spectrum. The strong feature in the Fourier transforms is due to the Se–O bond ($N = 3.7$, $r = 1.65$ Å). The parameters determined for Se–O were almost unchanged from the spectrum of a selenate solution, and were not influenced by the calculation accounting for the Se–Fe shell.

A clear peak for Fe–Se in the Fe K-edge Fourier transform and no significant contribution of the Se–Fe bond in the Se K-edge spectrum suggest that a large proportion of the selenate ions do not form a rigid Se–Fe bond, though all of them are strongly bound in the adsorption experiments. One possible explanation is that a considerable number of selenate ions are confined to the outer sphere of the Fe complex. The most likely average structure is that Fe is bound to one selenate at 3.28 Å and to one or zero Cl^- ions at 2.26 Å with 0.5 selenate ions in the outersphere. In this model, in order to neutralize the positive charge on the iron, the inner spherical selenate can be either $HSeO_4^-$ or SeO_4^{2-}.

EXAFS spectroscopic studies on selenate adsorption on goethite have yielded conflicting results: outersphere ($r = 3.38$ Å)[40] and bidentate innersphere ($r = 3.29$ Å)[41,42] complexes. On the other hand, both Raman and IR spectroscopies have indicated that both inner and outer sphere surface complexes of selenate and sulfate can occur on goethite and alumina.[43] Although a monatomic iron chelate complex is expected in the present system, the selenate–iron interaction in the adsorbed state shows the nature of both chemical bonds.

Conclusion

The adsorption of selenate occurs at the site of Fe^{3+}, Cu^{2+}, and H^+ cations anchored by diamino-functionalized MCM-41 with high distribution coefficients, K_d, and large capacities. K_d values of more than 200000 were observed at [selenate] < 25 mg for 1 g of these adsorbents. The adsorption capacities were 117, 83.0, and 123 mg (g-adsorbent)$^{-1}$, respectively. The Fe and Cu centers bound 1.5 and 1.1 selenate anions on average. Diamino-functionalized MCM-41 exhibited a larger K_d than mono- and triamino-functionalized MCM-41 when it was cationated by Fe^{3+} and Cu^{2+}. The inhibition of selenate adsorption by coexisting SO_4^{2-}, Cl^-, and NO_3^- was much lower than on aluminum oxide. Fe/ and Cu/NN-MCM-41 showed good resistance against inhibition by SO_4^{2-} and Cl^-, respectively. EXAFS spectra of the Fe and Se K-edges of Fe/NN-MCM-41 revealed a bond formation between Fe and Se at 3.27 Å.

References

1 C. T. Kresge, M. E. Leonovicz, W. J. Roth, J. C. Vartuli, and J. S. Beck, *Nature*, **710**, 359 (1992).

2 J. S. Beck, J. C. Vartuli, W. J. Roth, M. E. Leonowicz, C. T. Kresge, K. D. Schmitt, C. T.-W. Chu, D. H. Olson, E. W. Sheppard, S. B. McCullen, J. B. Higgins, and J. L. Schlenker, *J. Am. Chem. Soc.*, **114**, 10834 (1992).

3 T. Yanagisawa, T. Shimizu, K. Kuroda, and C. Kato, *Bull. Chem. Soc. Jpn.*, **63**, 988 (1990).

4 X. S. Zhao, G. Q. Lu, A. J. Whittaker, G. J. Millar, and H. Y. Zhu, *J. Phys. Chem. B*, **101**, 6525 (1997), and references therein.

5 X. Feng, G. E. Fryxell, L. Q. Wang, A. Y. Kim, J. Liu, and K. M. Kemner, *Science*, **276**, 923 (1997).

6 L. Mercier and T. J. Pinnavaia, *Environ. Sci. Technol.*, **32**, 2749 (1998).

7 J. Brown, R. Richer, and L. Mercier, *Microporous Mesoporous Mater.*, **37**, 41 (2000).

8 R. I. Nooney, M. Kalyanaraman, G. Kennedy, and E. J. Maginn, *Langmuir*, **17**, 528 (2001).

9 V. Antochshuk and M. Jaroniec, *Chem. Commun.*, **2002**, 258.

10 A. M. Liu, K. Hidajat, S. Kawi, and D. Y. Zhao, *Chem. Commun.*, **2000**, 1145.

11 H. Yoshitake, T. Yokoi, and T. Tatsumi, *Chem. Lett.*, **2002**, 586.

12 H. Yoshitake, T. Yokoi, and T. Tatsumi, *Chem. Mater.*, **14**, 4603 (2002).

13 H. Yoshitake, T. Yokoi, and T. Tatsumi, *Bull. Chem. Soc. Jpn.*, **76**, 847 (2003).

14 G. E. Fryxell, J. Liu, T. A. Hause, Z. Nie, K. F. Ferris, S. Mattigod, M. Gong, and R. T. Hallen, *Chem. Mater.*, **11**, 2148 (1999).

15 H. Yoshitake, T. Yokoi, and T. Tatsumi, *Chem. Mater.*, **15**, 1713 (2003).

16 K. V. Brix, D. G. Henderson, W. J. Adams, R. J. Robin, G. Richard, and D. O. McIntyre, *Environ. Toxicol.*, **16**, 142 (2001).

17 R. Yu, J. P. Coffman, V. van Fleet-Stalder, and T. G. Chasteen, *Environ. Toxicol. Chem.*, **16**, 140 (1997).

18 R. S. Ogle and A. W. Knight, *Arch. Environ. Contam. Toxicol.*, **30**, 274 (1996).

19 K. J. Maier, C. G. Foe, and A. W. Knight, *Environ. Toxicol. Chem.*, **12**, 755 (1993).

20 D. Wong and L. Oliveira, *Can. J. Fish. Aquat. Sci.*, **48**, 1193 (1991).

21 K. J. Buhl and S. J. Hamilton, *Arch. Environ. Contam. Toxicol.*, **30**, 84 (1996).

22 D. Peak and D. L. Sparks, *Environ. Sci. Technol.*, **36**, 1460 (2002).

23 P. Zhang and D. L. Sparks, *Environ. Sci. Technol.*, **24**, 1848 (1990).

24 M. Ike, K. Takahashi, T. Fujita, M. Kashiwa, and M. Fujita, *Water Res.*, **34**, 3019 (2000).

25 R. S. Oremland, J. S. Blum, A. B. Bindi, P. R. Dowdle, M. Herbel, and J. F. Stolz, *Appl. Environ. Microbiol.*, **65**, 4385 (1999).

26 D. T. Maiers, P. L. Wichlacz, D. L. Thompson, and D. F. Bruhn, *Appl. Environ. Microbiol.*, **54**, 2591 (1988).

27 S. J. Hamilton, K. J. Buhl, F. A. Bullard, and E. E. Little, *Environ. Toxicol.*, **15**, 48 (2000).

28 J. S. Ahlrichs and L. R. Hossner, *J. Environ. Qual.*, **16**, 95 (1987).

29 W.-H. Kuan, S.-L. Lo, M. K. Wang, and C.-F. Lin, *Water Res.*, **32**, 915 (1998).

30 S.-L. Lo and T.-Y. Chen, *Chemosphere*, **5**, 919 (1997).

31 H. Wijnja and C. P. Schulthess, *Soil Sci. Soc. Am. J.*, **64**, 1190 (2002).

32 R. P. J. J. Rietra, T. Hiemstra, and W. H. van Riemsdijk, *J. Colloid Interface Sci.*, **240**, 384 (2001), and references therein.

33 R. H. Neal and G. Sposite, *Soil Sci. Soc. Am. J.*, **53**, 70 (1989).

34 K. V. Brix, J. S. Volosin, W. J. Adams, R. J. Reash, R. G. Carlton, and D. O. McIntyre, *Environ. Toxicol. Chem.*, **20**, 1037 (2001).

35 M. J. Williams, R. S. Ogle, A. W. Knight, and R. G. Burau, *Arch. Environ. Contam. Toxicol.*, **27**, 449 (1994).

36 E. J. Boyle-Wright, L. E. Katz, and K. F. Hayes, *Environ. Sci. Technol.*, **36**, 1212 (2002).

37 A. N. Garg and P. N. Shukla, *Indian J. Chem.*, **12**, 996 (1974).

38 L. X. Chen, T. Liu, M. C. Thurnauer, R. Csencsits, and T. Rajh, *J. Phys. Chem. B*, **106**, 8539 (2002).

39 H. Sakane, I. Watanabe, K. Ono, S. Ikeda, S. Kaizaki, and Y. Kushi, *Inorg. Chim. Acta*, **178**, 67 (1990).

40 K. F. Hayes, A. L. Roe, G. E. Brown, K. O. Hodgens, J. O. Leckie, and G. A. Parks, *Science*, **238**, 783 (1987).

41 A. Manceau and L. Charlet, *J. Colloid Interface Sci.*, **218**, 289 (1999).

42 A. Manseau and L. Charlet, *J. Colloid Interface Sci.*, **168**, 87 (1994).

43 H. Wijnja and C. P. Shulthess, *J. Colloid Interface Sci.*, **229**, 286 (2000).